Electronic Supplementary Material (ESI) for RSC Applied Interfaces.

Electronic Supplementary Information

for

Ferrocene-labelled surfactants enhance the supercapacitor performance in PANI-PSS/nanocarbon layer-by-layer nanoarchitectonics electrodes

Ana Paula Mártire,[a] Gonzalo E. Fenoy, [a] Omar Azzaroni, [a] Matías Rafti, [a] Waldemar A. Marmisollé [a,] *

a. Instituto de Investigaciones Fisicoquímicas Teóricas y Aplicadas (INIFTA), Departamento de Química, Facultad de Ciencias Exactas, Universidad Nacional de La Plata, La Plata B1904DPI, Argentina.

* corresponding author: wmarmi@inifta.unlp.edu.ar

S1. Nanocarbon dispersion

The nanocarbon dispersion was prepared using expanded graphite (1 mg mL^{-1}) by probe sonication in deionized water in the presence of surfactant at 0.5 mg mL^{-1}. **Figure S1** shows the dispersion prepared **(left)** which had the same aspect for x=0, 0.5, and, 1. This dispersion was diluted 1:50 for preparing the assemblies. **Figure S1 (right)** shows a picture of the dilution.

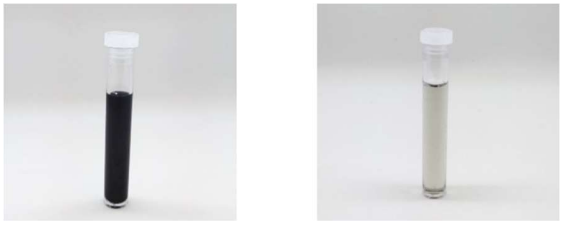

Figure S1. Picture of the nanocarbon dispersion (left) and the dilution prepared to do the assemblies (right).

S2. Raman Spectroscopy

To characterize the films, Raman spectroscopy measurements were performed with a BWTek Raman spectrometer (BWS415- 532S) equipped with an optical microscope (BAC151B model). The applied excitation wavelength was 785nm with a laser power of 50mW. The laser was focused on the sample using a 20x optical magnification. Au electrodes modified with an 11.5-bilayer assembly (x = 0, 0.5, and, 1), PANI-PSS, and nanocarbon dispersions, were measured (**Fig. S2**).

Typical PANI-PSS peaks are indicated in the graph. The signals at 810 and 1170 cm^{-1} are assigned to C-H bending in the quinoid and benzenic ring. The peak at 1255 cm^{-1} corresponds to the C-N stretching of the polaronic units. The 1340 cm^{-1} signal corresponds to the vibration of the semiquinone radical. Stretching corresponding to C=N and C=C were identified at 1486 and 1586 cm^{-1} respectively.[1] This peak description was observed in the spectra of the three different LbL assemblies. Peaks from the nanocarbon dispersion could not be identified in the assembly due to the superposition of these signals with the PANI-PSS ones and the intensity of the PANI Raman signal by the resonant Raman effect [2,3].

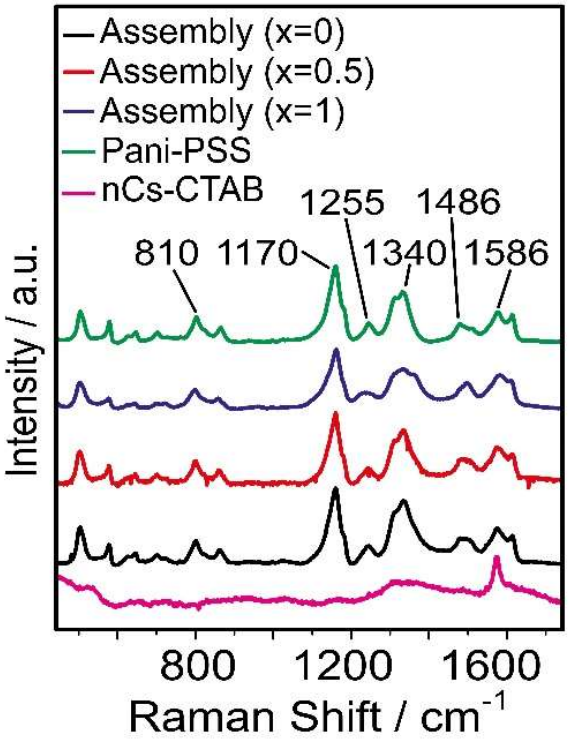

Figure S2. Raman spectra of the assemblies (x= 0, 0.5, and 1), PANI-PSS, and nanocarbon dispersions. The principal peaks identified in PANI-PSS are indicated in the graph.

S3. FTIR Spectroscopy

To evaluate the film composition FTIR spectroscopy measurements were carried out with a Nicolet Series FT-IR Spectrometer (Nicolet iS20). To compare the signals, Au electrodes modified with an 11.5-bilayer assembly (x = 0, 0.5, and, 1), PANI-PSS, and nanocarbon dispersions, were measured (**Fig. S3**). PANI-PSS and nanocarbon dispersion samples were prepared by drop casting over an Au surface dried overnight.

Coincidences between the nanocarbon dispersions and assembly spectrums were found. The peaks at 2920 and 2850 cm^{-1} (highlighted with yellow in **Fig.S3**) correspond to the -CH_2- asymmetric and symmetric stretching modes which come from the CTAB contribution.[4] Also, coincidences between PANI-PSS dispersion and the assemblies were found and highlighted with green in **Fig. S3**. Specifically, the peak at 1035 cm^{-1} from the symmetric stretching of the S=O binding from the PSS was identified in the assembly spectrums.[5,6] Next, signals from the aromatic ring of PANI and PSS were observed, at 1008 and 820 cm^{-1} related to in-place aromatic CH bending and out of plane aromatic CH deformation, respectively.[7,8] This result confirms the presence of the surfactant and PANI-PSS blocks within the assemblies.

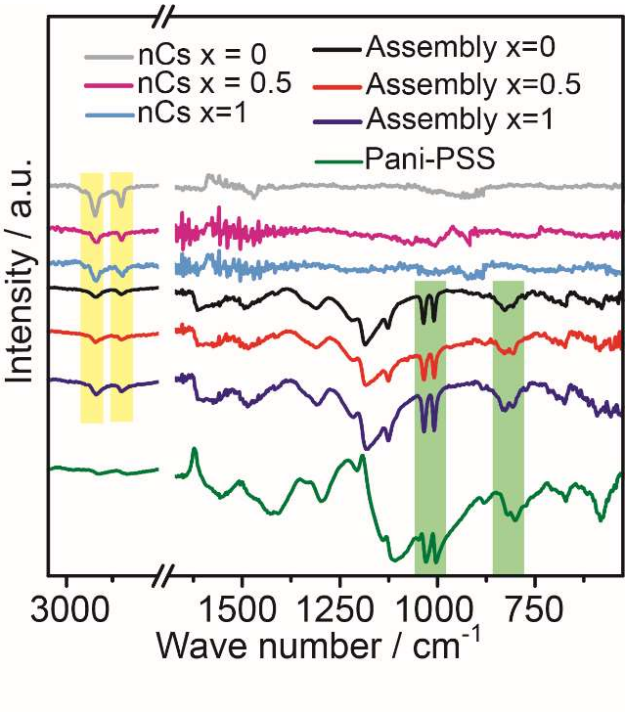

Figure S3. FTIR spectra of the assemblies (x= 0, 0.5, and 1), PANI-PSS, and nanocarbon dispersions. The principal coincidences with the nanocarbon and PANI-PSS dispersions are highlighted in yellow and green respectively.

S4. SEM Images

SEM images were captured in an environmental scanning electron microscopy (ESEM) FEI, Quanta 200 applying high vacuum to the samples. Au surfaces covered with 11.5 bilayer assembly of the three systems were observed. **Fig. S4** shows images taken of the three assemblies. A full covering with PANI-PSS film is observed in the three assemblies. The carbon contribution appeared as lighter blocks supported on the polymer matrix.

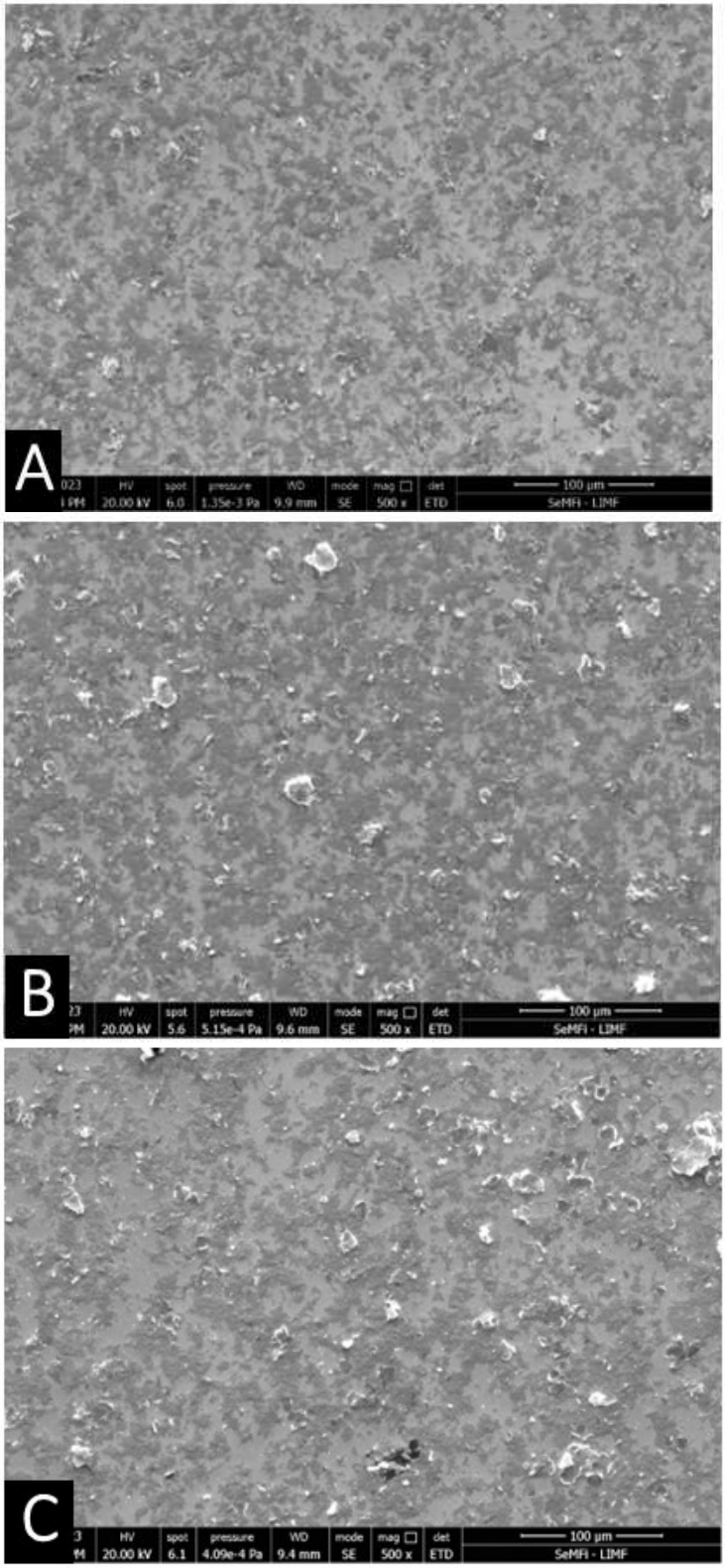

Figure S4. SEM images of the three 11.5 bilayer assemblies x= 0 (**A**), x= 0.5 (**B**), and x=1 (**C**).

S5. Effect of the presence of the nanocarbon

A control experiment was performed excluding the nanocarbon from the positive block dispersion. In this case, the assembly was prepared using the PANI-PSS dispersion, as the negative block, and only CTAB in the dispersion of the positive block. As reported in the main text, the assembly was performed directly in the electrochemical cell and cyclic voltammograms were recorded after a given number of deposition cycles. Voltammograms obtained revealed that the amount of electrochemically active material does not increase upon the successive deposition cycles in the absence of nanocarbon (**Fig. S4**) probing the role of the carbon material on the electrochemical connectivity and/or the LbL construction.

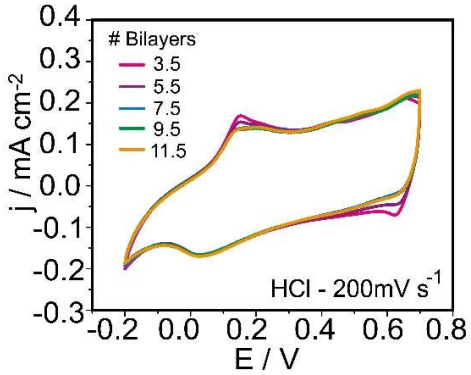

Figure S5. Cyclic voltammetry at 200mV s^{-1} in 0.1M HCl for the assembly without using the carbon component in the CTAB dispersion.

S6. Reproducibility of the LbL construction

Three identical experiments were performed to evaluate the reproducibility of the construction method. These replicates were produced by different nanocarbon dispersions and PANI-PSS synthesis batches. The average specific capacitance of these electrodes increases with the proportion of ferrocene-labelled surfactant included in the assembly (**Fig. S5**). The variability in the capacitance values is attributed to batch-to-batch differences in the preparation of the building blocks and the assembly process of the supramolecular units.

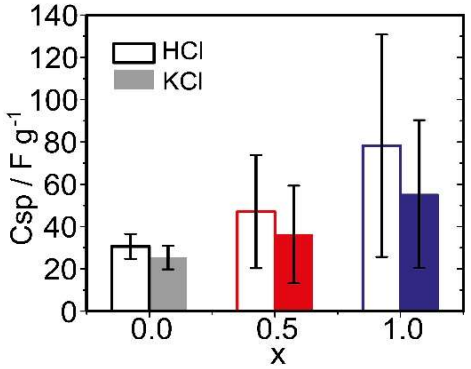

Figure S6. Specific capacitance at 200 mV s^{-1}. Average from three different preparation sets (N=3). Bars correspond to the standard deviation.

S7. Zeta potential measurement

Zeta potential measurements were carried out in a ZetaSizer Nano (Nano ZSizer-ZEN3600, Malvern, U.K.). Disposable capillary cells (DTS 1061 1070, Malvern) were used at 25°C. The zeta potential value was obtained from the electrophoretic mobility measured by laser Doppler velocimetry with a drive cell voltage of 30 V and employing the monomodal analysis method.

Zeta potential of the PANI-PSS dispersion determined in 0.5M HCl was -13.8 mV. A second measurement was carried out in PANI-PSS dispersion at pH 7. For this purpose, the dispersion was neutralized adding 10% KOH. The obtained zeta potential of the PANI-PSS dispersion at pH 7 was -21.6 mV.

S8. Mass exchange during cyclic voltammetry

QCM Au sensors were modified by the same procedure explained in **Scheme 1**. These electrodes were used to determine the increment of the mass after different number of deposition cycles (**Fig. 4A**). The exchange of ions during the electrochemical cycling was studied using a QCM SRS 200 and Gamry potentiostat in combination. **Fig. S7** shows the result obtained for the electrode x = 0.5 cycled in 0.1M HCl at 10 mV s^{-1}.

The Sauerbray model was employed to calculate the mass exchange [9,10]. Voltammograms in **Fig. 4** and **Fig. S7** were integrated to calculate the voltammetric charge. The ratio between the mass and the charge was determined to calculate the molar mass of the exchange species (**Table S1**)[11]. The molar mass of the exchanged species determined in 0.1M KCl was greater than those in 0.1M HCl. The average values obtained were 136 and 21.5 g mol^{-1} in KCl and HCl, respectively.

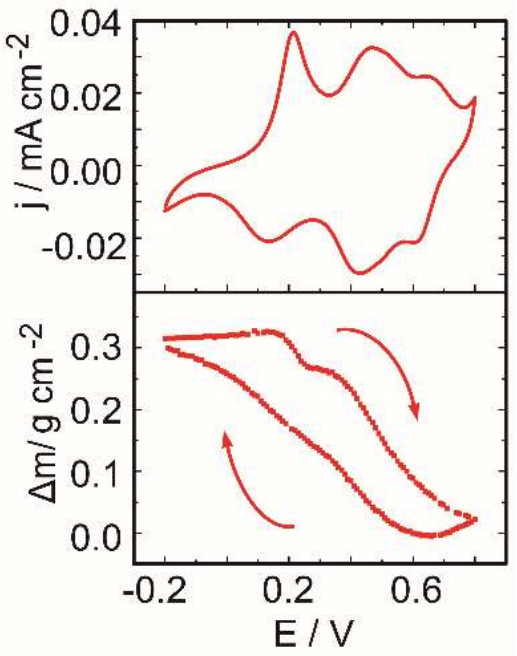

Figure S7. Mass change curves and cyclic voltammetry of QCM electrodes at 10 mV s^{-1} in 0.1M HCl for x = 0.5.

Table S1- Molar mass results of the exchanged species during cyclic voltammetry.

		Equivalent molar mass of the exchanged species (g mol^{-1})			
Process / Sample		KCl (x=1)	KCl (x=0.5)	KCl (x=0)	HCl (x=0.5)
Oxidation	1st	81	171	144	19
	2nd	107	144	83	24
Reduction	1st	168	208	174	22
	2nd	75	111	170	21

S9. GCD curves

The three 11.5-bilayer systems with different proportion of the ferrocene-labelled surfactant were compared in terms of the charge-discharge galvanostatic performance **Fig. S8A** compares their performance in 0.1M KCl at 1 Ag^{-1}. **Fig. S8B** presents the relative specific capacity for these three systems in 0.1M KCl and 0.1M HCl referred to *x*=0 values (C_0).

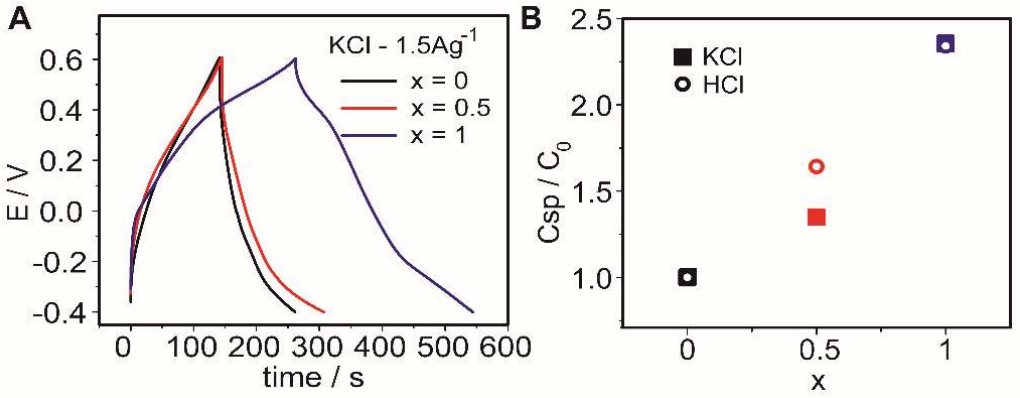

Figure S8. Charge and discharge cycles for assemblies with different x values in 0.1M KCl (**A**) Relative specific capacitance for different *x* values for charge-discharge cycles in 0.1M HCl and 0.1M KCl (**B**).

S10. Voltammetric stability

The stability test towards continuous voltammetric cycling for *x*=0 and *x*=0.5 11.5-bilayer electrodes is shown in **Fig. S9**. Up to 100 cycles were performed in 0.1M KCl at 200mV s^{-1}. The integrated voltammetric charges from these voltammograms are reported in **Fig. 6B**. No significant variations in the voltammetric

stability was observed among the assemblies with different proportion of the ferrocene-labelled surfactant during 100 consecutive cycles.

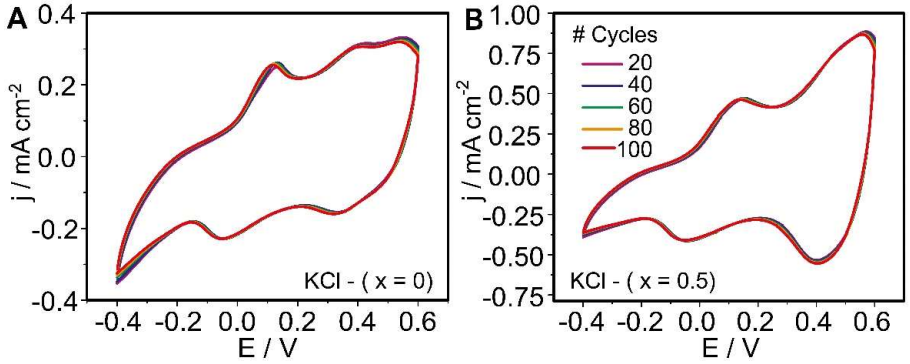

Figure S9. Cyclic voltammograms for 100 cycles for x=0 (**A**) and x=0.5 (**B**) in 0.1M KCl at 200 mV s^{-1}.

References

1 G. E. Fenoy, B. Van der Schueren, J. Scotto, F. Boulmedais, M. R. Ceolín, S. Bégin-Colin, D. Bégin, W. A. Marmisollé and O. Azzaroni, *Electrochim. Acta*, 2018, **283**, 1178–1187.

2 A. C. Ferrari and D. M. Basko, *Nat. Nanotechnol.*, 2013, **8**, 235–246.

3 L. G. Cançado, A. Jorio, E. H. M. Ferreira, F. Stavale, C. A. Achete, R. B. Capaz, M. V. O. Moutinho, A. Lombardo, T. S. Kulmala and A. C. Ferrari, *Nano Lett.*, 2011, **11**, 3190–3196.

4 W. Xue, H. He, J. Zhu and P. Yuan, *Spectrochim. Acta Part A Mol. Biomol. Spectrosc.*, 2007, **67**, 1030–1036.

5 C. R. Martins, G. Ruggeri and M.-A. De Paoli, *J. Braz. Chem. Soc.*, 2003, **14**, 797–802.

6 R. A. Weiss, A. Sen, C. L. Willis and L. A. Pottick, *Polymer (Guildf).*, 1991, **32**, 1867–1874.

7 Z. Ping, G. E. Nauer, H. Neugebauer, J. Theiner and A. Neckel, *Electrochim. Acta*, 1997, **42**, 1693–1700.

8 V. F. Kalasinsky and T. S. Little, *J. Raman Spectrosc.*, 1980, **9**, 224–229.

9 Gyorgy Inzelt, in *Electroanalytical Methods: Guide to experiments and applications*, ed. F. Scholtz, Springer Berlin Heidelberg.

10 M. R. Deakin and D. A. Buttry, *Anal. Chem.*, 1989, **61**, 1147A-1154A.

11 E. Piccinini, G. A. González, O. Azzaroni and F. Battaglini, *J. Colloid Interface Sci.*, 2021, **581**, 595–607.